

Low velocity impact performance of recyclable all-polypropylene composites

B. Alcock ^{a,*}, N.O. Cabrera ^{a,b}, N.-M. Barkoula ^a, T. Peijs ^{a,b}

^a Department of Materials, Queen Mary, University of London, Mile End Road, London E1 4NS, UK

^b Eindhoven Polymer Laboratories, Eindhoven University of Technology, P.O. Box 513, 5600 MB, Eindhoven, Netherlands

Received 1 July 2005; received in revised form 5 November 2005; accepted 7 November 2005

Available online 3 January 2006

Abstract

Highly oriented polypropylene (PP) tapes, with high tensile strength and stiffness achieved by molecular orientation during solid state drawing are consolidated to create high performance recyclable “all-polypropylene” (all-PP) composites. These composites possess a large temperature processing window (>30 °C) and a high volume fraction of highly oriented PP (>90%). This large processing window is achieved by using co-extruded, highly drawn PP tapes. This paper investigates the impact resistance of these all-PP composites, and the relationship between penetrative and non-penetrative impact behaviour, and composite consolidation conditions. The response of all-PP composites to falling weight impact is reported together with a comparison to conventional commercial glass reinforced polypropylene composites. A model for energy absorption is proposed by comparison with previous studies based on interfacial and tensile failure of tapes and composites.

© 2005 Elsevier Ltd. All rights reserved.

Keywords: B. Interface; B. Impact behaviour; A. Recycling; C. Delamination; A. Fabric/Textiles

1. Introduction

All engineering structures are susceptible to impact loading within their service lives. The response of the material to impact loading will depend on various factors such as the geometry of the structure and striker, the mass and velocity of the striker, and frequency of impacts. Due to their high strength and stiffness, and good energy absorption due to delaminating failure modes, composite materials generally perform well in impact applications. Carbon and glass fibres suffer from a lack of plasticity which means that non-penetrative impact loads can lead to (often invisible, subsurface) fibre damage, which can drastically reduce the residual mechanical properties of the composite [1]. Thermoplastic fibre composites typically possess sufficient elastic limits to make them less sensitive to damage from lower energy impacts [2] (see Table 1).

Thermoplastic fibres such as UHMW-PE (e.g., Dyneema[®], DSM, or Spectra[®], Honeywell) have specific applications as impact defence materials, such as personal protection for military/police personnel from direct projectile impact [3], or as spall liners behind ceramic/metallic armour in armoured vehicles to limit proliferation of shrapnel inside a vehicle following impact [4].

Composite ballistic protection can also provide significant weight savings for automotive defence, compared to steel armour [5,6] and has also been assessed as fragment barriers for commercial aircraft [7]. The impact performance of composites has been modelled with some success to determine the methods of predict deformation [8] and model energy absorption [9].

1.1. All-polypropylene composite processing

In a series of PhD theses [10–12], novel composite materials in which both the fibre and the matrix are based on polypropylene (PP) have been described. The creation of single

* Corresponding author.

E-mail address: b.alcock@gmail.com (B. Alcock).

Table 1
Typical fibres properties for a range of commonly used fibre reinforcements for impact applications

Material	Fibre type	Tensile strength (MPa)	Tensile modulus (GPa)	Strain to failure (%)	Density (g cm ⁻³)	Reference
PBO	–	5.5	280	2.5	1.56	[3]
Glass	E Glass	3.5	72	4.8	2.58	[50]
	S-2 Glass	4.9	87	5.7	2.46	[50]
Aramid	<i>Twaron HM1055</i>	2.8	125	2.5	1.45	[51]
	<i>Twaron HS2000</i>	3.8	90	3.5	1.44	[51]
	<i>Kevlar 49</i>	2.9	135	2.8	1.45	[51]
	<i>Kevlar 129</i>	3.4	99	3.3	1.45	[51]
UHMW-PE (Gel processed)	<i>Dyneema SK60</i>	2.7	89	3.5	0.97	[52]
	<i>Dyneema SK71</i>	4.0	120	4.1	0.97	[52]
	<i>Spectra S900</i>	2.1	79	3.6	0.97	[52]
	<i>Spectra S2000</i>	3	116	2.9	0.97	[52]
UHMW-PE (Melt processed)	<i>Certran</i>	1.2	67	6	0.97	[53–55]
UHMW-PP (Gel processed)	–	0.98	36	3.3	0.91	[56]
PP	All-PP tapes	0.45	15	7.5	0.78	[11]

polymer composites is motivated by the desire to enhance recyclability of composite materials. Conventional composite employ very different materials for the matrix and reinforcement phase and this complicates recycling. All-PP composites overcome this problem since at the end of the life of an all-PP product, the entirely polypropylene composite can simply be melted down for reuse in a PP feedstock or even in a subsequent generation of all-PP composite.

While neither the concept of creating high modulus polymer fibres [13–23] or single polymer composites are new [24–33], existing technologies have inherent limitations such as a relatively small temperature processing window or a low volume fraction of reinforcement, which limit the ultimate mechanical properties of the composites. Highly oriented, high modulus fibres or tapes can be effectively welded together by melting the surface of the tapes and applying pressure to achieve a good bonding and fill any voids [33–36]. In these mono-extruded tape or fibre systems, the process becomes highly sensitive to compaction temperature, since there is a risk of molecular relaxation during the high temperature consolidation of tapes or fibre bundles into composites.

The research reported in this paper focuses on the use of co-extruded tape technology to create all-PP composites with a large temperature processing window (>30 °C) and high volume fraction of reinforcement (>90%). The large temperature processing window of these co-extruded tapes allows all-PP composite production over the range of this temperature processing window by providing enough thermal energy to allow consolidation of tapes into a load bearing structure but without significant loss of mechanical properties. This does not imply that all mechanical properties are uniform over this temperature window. The effect of compaction temperature and pressure on the mechanical properties of all-PP composites is discussed in great detail elsewhere [37,38]. These co-extruded tapes possess a skin-core morphology and are composed of a core of PP homo-

polymer sandwiched between a thin skin of a PP copolymer. This three-layer structure is co-extruded in a high viscosity melt phase and subsequently drawn in a two stage solid state drawing process also described in greater detail elsewhere [11,22,39]. This drawing process results in a high degree of molecular orientation and the drawn tapes possess a high tensile strength (>450 MPa) and stiffness (>15 GPa). These co-extruded tapes can then be consolidated into a composite material by the application of heat and pressure to stacked plies of woven tape fabrics [12,37,39]. The application of pressure also causes a physical constraining effect which has been shown to artificially raise the melting temperature of highly oriented polymers [22,40,41], and this effect further helps to retain the tensile properties in the tapes by preventing molecular relaxation during consolidation. The copolymer skin layer possesses a lower melting temperature than the homopolymer core and hence allows tapes to be effectively welded together at temperatures far below the melting temperature of the homopolymer core. The proportional thickness of the skin to the core can be altered during co-extrusion, but since the skin layer is present only to facilitate intertape bonding, it is desirable to have this skin as thin as possible while achieving a high interfacial strength. The mechanical properties of these tapes together with the inherent low density of PP, and the high volume fraction of reinforcement present in these composites ($V_f > 90\%$) make these all-PP composites competitive with conventional PP matrix composites [12,37,39]. Since the PP tapes used in this research are co-extruded, the matrix phase (skin layer) is carried by the core layer, in one tape. The optimisation of both the homopolymer (reinforcement) layer for high mechanical properties and the copolymer (matrix) layer for good interfacial strength must be considered simultaneously. While the extrusion and solid state drawing parameters determine the mechanical properties of these tapes, the same parameters also affect the morphology of

the copolymer layer strength of the interfaces formed when these tapes are bonded to each other in a composite system. Energy absorption during impact is achieved by a variety of failure modes, predominantly a combination of fibre failure and interfacial failure. Since composite consolidation parameters control both the interfacial properties and the mechanical properties in woven tape all-PP composites, it is important to investigate how composite consolidation parameters affect the impact performance of all-PP composites [11].

This paper aims to investigate the impact energy absorption by woven tape all-PP composites, processed with a range of processing conditions. By comparing the energy absorbed during pure interfacial failure with energy absorbed during pure tensile failure of tapes, a model is proposed which can be used to predict the impact performance of all-PP composites. The temperature and impact velocity are kept constant in the experiments presented in this paper, since the viscoelastic nature of polymeric systems means that these factors are likely to effect impact energy absorption.

1.2. Materials

To illustrate the versatility of all-PP composites, two types of co-extruded tapes will be used for composite production. Three-layer (skin:core:skin) tapes are co-extruded and drawn in a solid state drawing process as described in Table 2. In this way, the material which will comprise the matrix phase is present in the tapes as a thin 'skin' on the top and bottom of the reinforcement phase, the 'core' of the tape. Both of these tapes are composed of the same polymers and only subjected to different drawing conditions. Both tapes consist of a PP homopolymer blend core layer ($M_w = \sim 300 \text{ kg mol}^{-1}$, $\text{MFI} = 5 \text{ g min}^{-1}$) co-extruded with a copolymer skin layer ($M_w = 320 \text{ kg mol}^{-1}$, $\text{MFI} = 5.5 \text{ g min}^{-1}$). Following co-extrusion, the tape is drawn with parameters described in Table 2, to yield two kinds of tape designated A and B which are woven into fabrics A and B, respectively. During solid state drawing, molecular orientation and so high mechanical properties are achieved depending on draw ratio applied, and after drawing the tapes typically have a width of 2 mm and a thickness of 65 μm .

All-PP fabric A is composed of a high draw ratio tape, with high tensile modulus, high strength and a relatively poor interfacial strength. Fabric B is composed of a lower draw ratio tape with a lower tensile modulus and strength but a stronger interfacial strength. The interfacial strengths

were characterised using single tape T-peel tests (ASTM 1876) [11] and will be described in greater detail in a dedicated publication. These processing characteristics affect mechanical and interfacial properties and so greatly affect failure modes. By using two different fabrics, the range of properties achievable with all-PP composites is demonstrated, as is the strong link between tape processing properties and composite properties, allowing user-definable tape properties to control ultimate composite properties.

1.3. Specimen preparation

Penetrative falling weight impact testing employs laminates of material which are subjected to impact normal to the plane of the laminate as shown in Fig. 1. The production of all-PP laminates will now be described. Co-extruded all-PP tape is woven into a plain weave fabric with an areal density of $\sim 100 \text{ g m}^{-2}$. This fabric is cut into square plies and placed in close fitting mould with dimensions of $180 \times 180 \text{ mm}$. This mould can then be placed in a hot press and heat ($130\text{--}170 \text{ }^\circ\text{C}$) and pressure ($1\text{--}12 \text{ MPa}$) can be applied. Alternatively, this mould can be consolidated in a vacuum bag while heated in an oven to achieve temperatures of $130\text{--}150 \text{ }^\circ\text{C}$ and pressure of $0.1\text{--}1 \text{ MPa}$. In either case, temperature in the mould is monitored using externally monitored PT100 temperature probes, and temperature across the mould was seen to be uniform within $1 \text{ }^\circ\text{C}$; this is crucial since maintenance of high mechanical properties depends on accurate temperature control. The application of lateral pressure by either a hot press or a vacuum oven acts to physically constrain the fabrics and prevents relaxation during heating [22,40,41]. Upon cooling, pressure is removed and consolidation of the composite is complete. The all-PP composite can then be removed from the mould. A range of consolidation temperatures and pressures was investigated to determine the effect that these had on impact performance.

In addition to mechanical properties, composite density also varies with compaction parameters. With increasing compaction pressure and temperature, superior consolidation of fabric plies is achieved and so the apparent density of the composite laminates increases by the closure of interply voids. For this reason, this paper often refers to specific mechanical properties, i.e., mechanical properties proportional to density. For example, a poorly compacted specimen may appear to have a lower tensile modulus, but this may be due to a higher volume fraction of interply voids giving a falsely low density and hence an inaccurate measure of material dimensions, rather than molecular relaxation (and so a reduction in modulus) of the constituent tapes.

2. Experimental procedure

2.1. Penetrative falling weight impact testing

Falling weight impact testing can provide analytical information about the mechanism on impact such as spec-

Table 2
Details of all-PP fabrics A and B

Fabric	Tape draw ratio (λ)	Tape modulus (GPa)	Tape strength (MPa)	Relative tape composition (skin:core:skin)	Drawing temperature ($^\circ\text{C}$)
A	17	15	450	5:90:5	170
B	8	6	300	10:80:10	160

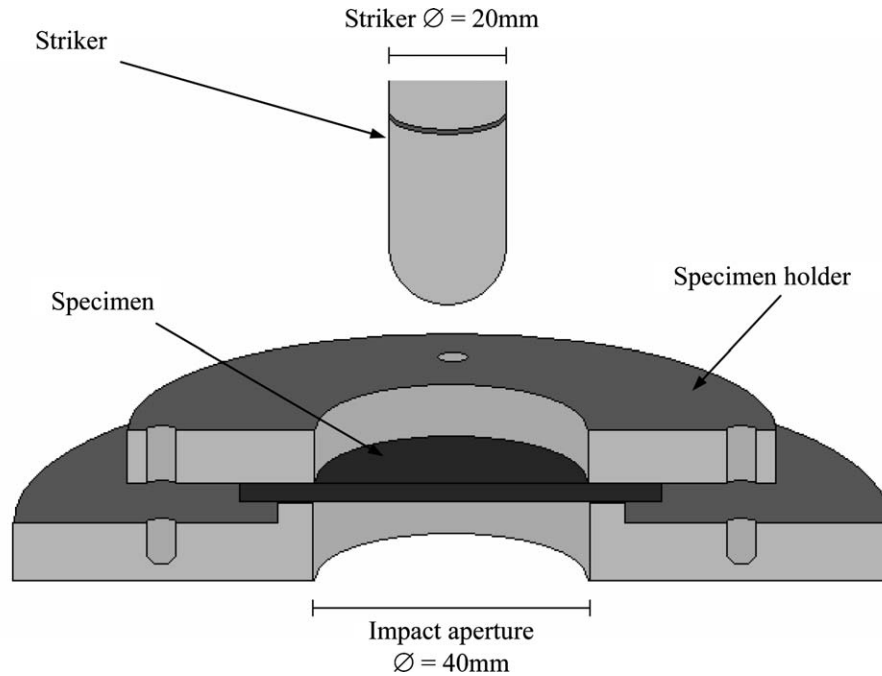


Fig. 1. Schematic of falling weight impact test set-up.

imen displacement, duration of impact and energy absorption, but are limited to lower velocities, $<10 \text{ m s}^{-1}$. The ballistic energy absorption of all-PP composite laminates has been investigated by impacting laminates at much greater velocities ($>250 \text{ m s}^{-1}$) and these results will be presented elsewhere. Penetrative falling weight impact tests were performed as described by ASTM 5628-96 (using ASTM geometry 'FE'), on a range of woven all-PP composite plates. The falling weight impact test machine used is manufactured by Ceast, Italy, and has a 10 mm radius hemispherical striker suspended at a measured height which, upon release, falls freely to strike the specimen fixed in a circular aperture beneath. A cut away schematic of the impact aperture is shown in Fig. 1.

The impact striker contains a force transducer which measures the force upon impact, and this force/time provides a measurement of the energy absorbed by the impact [42]. The force/time curve is first integrated, to give the area under the curve, A_{total} [43]:

$$A_{\text{total}} = \int_0^{\infty} F(t) dt. \quad (1)$$

And then energy absorbed by impact, E_{impact} can be calculated by

$$E_{\text{total}} = v_0 \times A_{\text{total}} \left(1 - \frac{v_0 A_{\text{total}}}{4E_S} \right), \quad (2)$$

where E_{total} = total energy of impact, v_0 = impact velocity, A_{total} = area under force/time curve and E_S = energy of striker. It is possible to alter the energy of the striker by varying the initial height or the mass on the striker. In these tests, height is kept constant at 1 m and mass is varied in order to vary impact energy while maintaining constant im-

act velocity. For penetrative impact tests, the initial energy is always at least twice the energy absorbed in penetration in order to increase measurement accuracy. Energy losses due to friction in falling, sound, and heat are negligible, so will be ignored.

2.2. Non-penetrative falling weight impact testing

Non-penetrating impact tests were performed to investigate the mechanisms of impact damage on all-PP plates. Tests were performed on a similar Ceast falling weight impact machine with an identical striker, but also equipped with a mechanism to catch the striker on rebound from initial impact, and prevent further strikes which occur following rebound from non-penetrating impact. The impact energy was kept constant at 20 J. Prior to testing, specimens were airbrushed with a fine, random, high contrast speckle pattern. High resolution images of these surfaces were captured using an ARAMIS 3D strain mapping system manufactured by GOM GmbH (Germany), equipped with two Vosskühler CCD 1300F high resolution digital cameras [44]. Following impact, images of the specimens were captured again, and the ARAMIS software can produce a three dimensional map of the surface deformation due to impact damage. This requires the speckle pattern to remain intact during impact, and so complete maps cannot be produced if the surface layer is damaged or the pattern is removed by abrasion with the impact striker or gripping mechanism. The application of digital surface strain mapping has been successfully applied to bi-directional thermoplastic composites undergoing similar deformation due to stamping rather than non-penetrative impact [45] and has been applied to the thermoforming

of all-PP composites elsewhere [12]. A more traditional method for assessing damage in non-penetrating impact of composites is ultrasonic C-scan, but as this method relies on varying densities within a fluid medium, typically water, it cannot easily be applied for a material such as polypropylene with a density so close to the density of water, 1 g cm^{-3} . The acoustic damping and the lack of large scale delaminations of tough materials such as polypropylene also reduce the efficiency of ultrasound scanning methods.

2.3. T-peel interfacial characterisation

To determine the effect of temperature of intertape bonding of individual tapes, T-peel tests are performed in accordance with ASTM 1876; peeling of a pair of compacted tapes is performed in a Hounsfield HK25S tensile testing machine fitted with a 5 N load cell, appropriate grips and data acquisition software. The crosshead displacement causes two bonded tapes to peel apart at 180° in a mode I failure. The tests were performed at crosshead displacement of 5 mm min^{-1} , and each test was repeated at least five times to ensure reproducibility. The values presented for peel force are defined as the force per unit width of tape required to peel the tapes apart, since this tends to a constant value during peeling.

3. Results and discussion

3.1. Penetrative impact performance

Due to the dimensional effect of processing conditions on the compaction of all-PP specimens, as discussed elsewhere [11], it is important to determine the geometrical effect due to different specimen dimensions on the impact performance. Fig. 7 shows the effect of specimen thickness on penetrative impact resistance for two different all-PP composites composed of fabrics A and B, with a woven glass-PP for comparison. As described in [11], fabric B is woven from a tape with a lower draw ratio, and so greater ply thickness. This leads to a greater thickness for the same number of plies compared to fabric A. Fig. 2 also shows a comparison of thickness with number of plies (shown in brackets). For specimens less than 2 mm thick, there is clearly a non-linear relationship between specimen thickness and penetrative energy for all-PP composites.

This is explained by examining the force–time curves of the impact penetrations for different thickness of all-PP composites. Fig. 3 shows four typical force–time curves for fabric A. For thicker specimens, behaviour is very similar, with maximum force increasing with specimen thickness. For specimens with a thickness of 1.2 mm, a greater time to reach maximum force is observed. This is due to increased deflection of the specimen upon impact; very thin specimens exhibit greater flexural deformation. This will lead to a greater impact duration and a greater energy absorption, and so very thin specimens show a disproportional penetrative energy compared to their relative thick-

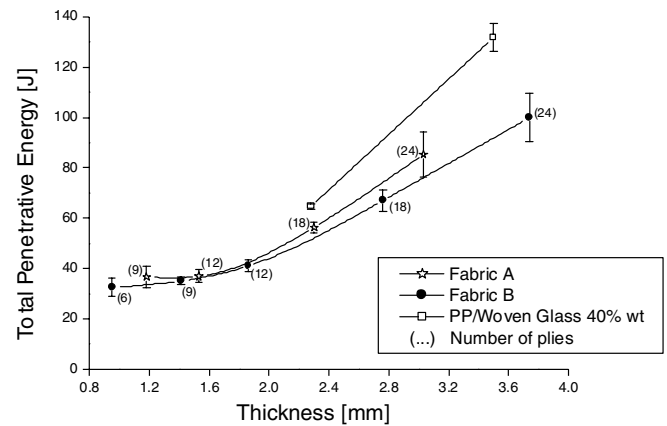


Fig. 2. Absorbed penetrative impact energy vs. specimen thickness for different all-PP and a commercial woven glass reinforced PP composite showing a non-linear relationship between specimen thickness and absorbed energy.

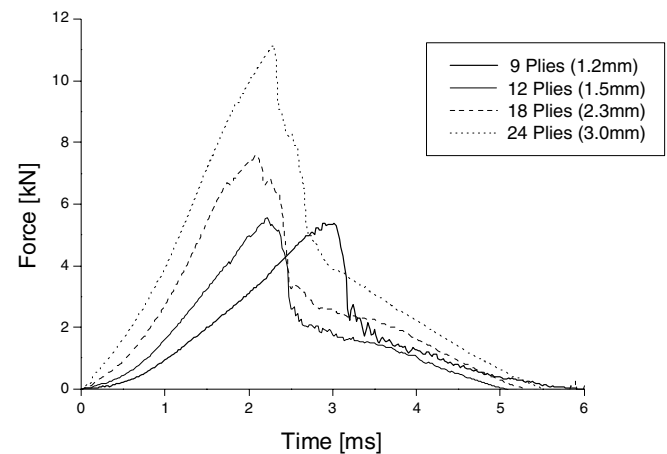


Fig. 3. Force vs. time curves of typical all-PP composites with varying thickness showing an increase of impact time with 1.2 mm thick specimens indicating greater deflection during impact.

ness (see Fig. 4). Considering this non-linearity, all further impact tests are performed on specimens of greater than, but close to 2 mm thickness, so that thickness can be normalized in the approximately linear region of the impact energy/thickness relationship. In any case, the impact performance of the all-PP composites described in this study can be considered a minimum performance, since this rather high thickness of all-PP composites gives the lowest impact performance.

Previous studies [12,37,39] have shown that the mechanical properties of all-PP composites are determined by processing parameters and this is also true of impact energy absorption. Fig. 5 shows the effect of compaction temperature and pressure on the specific tensile strength and specific tensile modulus of all-PP composites. The specific properties are defined as the property in question (i.e., tensile modulus or strength) divided by density. Since processing conditions alter composite density by affecting interply void closure, it is important to isolate the effect of process-

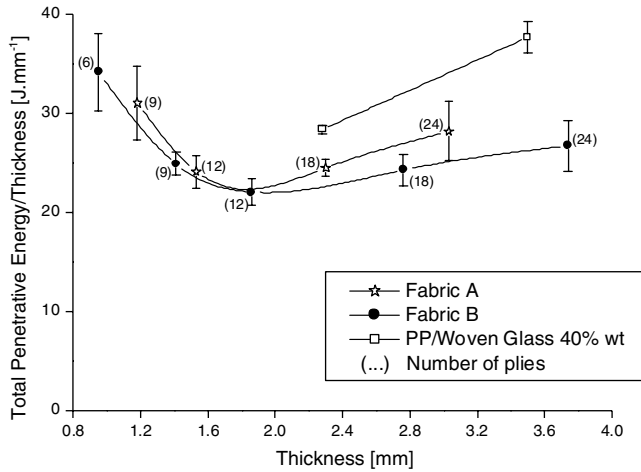


Fig. 4. Impact energy normalised for specimen thickness vs. specimen thickness indicating a large impact energy/thickness absorbed by the thinnest specimens.

ing conditions on mechanical properties of the constituent tapes. Fig. 6 shows the effect of compaction temperature on the impact resistance of all-PP plates (compaction pressure is constant at 1 MPa for each all-PP specimen shown in this graph), compared to PP strengthened with ‘foreign’ reinforcements: woven glass reinforced polypropylene (Twin-tex®, Saint Gobain-Vetrotex, 40% wt.), glass-mat reinforced polypropylene (GMT, Symalite®, Quadrant Composites, 23% wt.) and flax fibre reinforced polypropylene (NMT, 40% wt.). These traditional composites are represented as horizontal lines even though impregnation/consolidation are not necessarily viable across this temperature window. For both all-PP fabrics, there is a general decrease in absorbed impact energy with increasing compaction temperature.

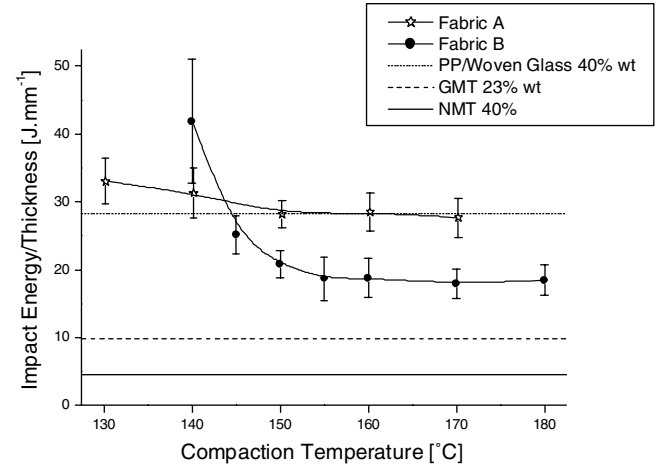


Fig. 6. Impact energy vs. compaction temperature for two all-PP fabrics and some common reinforced PP alternatives. While both all-PP fabrics perform very well in impact, fabric B shows impact behaviour which can be controlled by compaction temperature and fabric A shows a much more constant impact behaviour over a wide range of compaction temperatures.

As the tensile strength of woven all-PP composite plates processed at the same compaction pressure is largely independent of compaction temperature within the range of temperatures shown here [37], the change in absorbed impact energy with compaction temperature can be traced to changes in the interfacial strength. Fig. 7 combines the absorbed impact energy of fabrics A and B with adhesive strength determined from T-peel tests of single tapes of A and B. These properties are clearly linked, with impact strength being inversely related to the interfacial strength of the tapes.

At lower compaction temperatures, the interface is weaker and so tape debonding is the preferential mechanism of impact failure. This delamination, together with

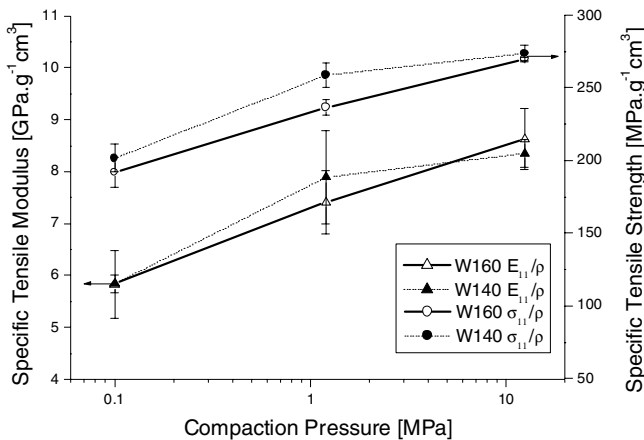


Fig. 5. Specific tensile properties of woven fabric A all-PP laminates vs. compaction pressure during laminate production, in which W140 and W160 refer to woven tape all-PP specimens compacted at 140 °C and 160 °C, respectively, and E_{11} and σ_{11} are tensile modulus and tensile strength, respectively. This shows that specific mechanical properties are controlled by applied compaction pressure during laminate production. There is a negligible effect of compaction temperature in the range of temperatures presented here. Reproduced from [11].

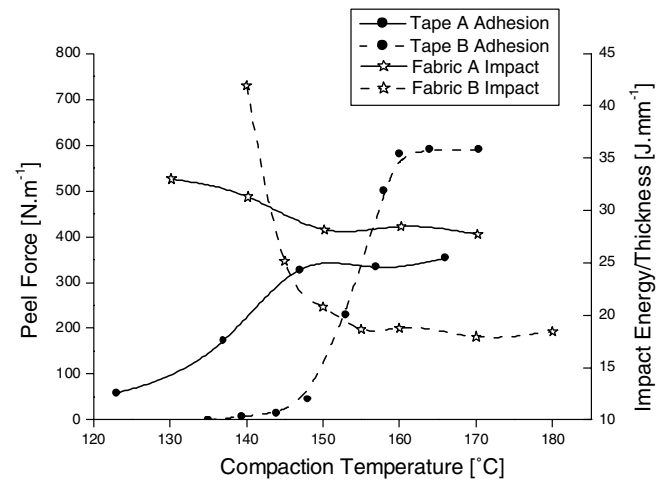


Fig. 7. Peel force vs. impact energy for two different all-PP composites showing the relationship between interfacial strength (determined by T-peel testing of single tapes) and impact energy absorption. It can be clearly seen that as interfacial strength increases, impact energy absorption decreases.

fibrillation and tape pull-out are highly energy consuming processes. As compaction temperature is increased, the interface becomes stronger and so the dominant mechanism of failure appears to be tape failure very locally to the impact site. Thus at lower compaction temperatures, as the interface is weaker, the energy absorbed is less localised and the absorbed impact energy is greater [9,46]; the same effect has been reported for hot compacted gel-spun UHMW-PE fibres composites [47]. As in interfacial studies described elsewhere [11] and described in future publications, because the effect of processing temperature of fabric A is much less than that of fabric B (see Figs. 6 and 7), the effect of temperature on absorbed impact energy is much less dramatic in fabric A than fabric B. This also makes fabric A a more easily processable and consistent material for consistent impact resistance, and so is preferred for ease of processing. It has now been shown that impact performance can be varied by altering tape processing parameters such as draw ratio, as well by altering composite processing. For clarity

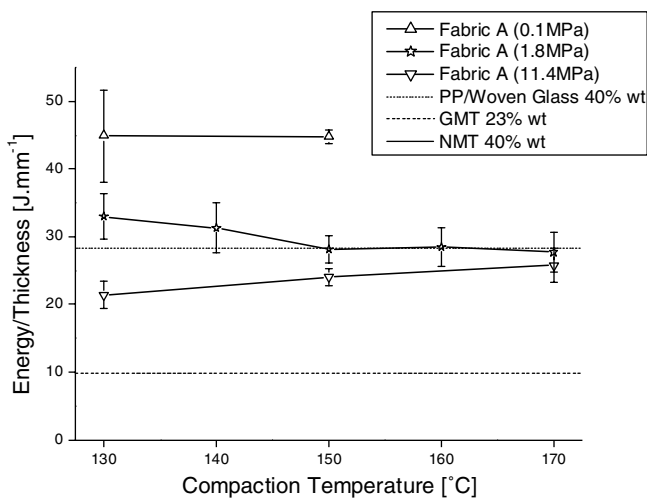


Fig. 8. The influence of compaction pressure and temperature on impact energy revealing that all-PP laminates consolidated with the lowest compaction pressure absorb the largest impact energy.

from this point forward, the results presented shall be based on tests performed on fabric A.

As with the tensile properties, the pressure at which the all-PP composites are compacted also affects impact properties. Fig. 8 shows the effect of compaction pressure on the impact performance of fabric A, again with woven glass PP, GMT and NMT for comparison. The all-PP specimens have been compacted at three different pressures of 0.1 MPa (via a vacuum bagging processing route), 1.8 and 11.4 MPa (via a hot pressing route) as described earlier. Here it is clear that all-PP composites can easily compete on impact performance with the woven glass PP tested. As compaction pressure of the all-PP composites increases, absorbed impact energy is reduced even when normalised for the decreasing thickness which accompanies processing at elevated pressures. This is due to an increase in interfacial strength with increasing compaction pressure, as seen before for increasing compaction temperature. At all compaction pressures, an almost constant absorbed impact energy is seen over the range of temperatures tested.

Due to the relatively low density of bulk PP and even lower density of all-PP composites (see Table 3), these composite plates perform very well when specific impact energy (normalised for density) is taken into account. Fig. 9 shows the specific performances of these all-PP plates compared to woven glass PP, GMT and NMT, all normalised for density. From these results, all of the all-PP plates out-perform each of the alternatives considered here (see Table 3).

The transition in failure mode can be most clearly seen in post impact specimens which have been compacted at different temperatures and pressures (see Fig. 10). By comparing an all-PP plate which has been compacted at a low temperature and low pressure (140 °C, 0.1 MPa), with an all-PP plate which has been compacted at a high temperature and high pressure (160 °C, 11.4 MPa), the energy absorption mechanisms of plates which exhibit the highest and lowest impact energy absorption, respectively, can be investigated. Fig. 10a shows an impacted specimen which has been compacted at low temperature and pressure (140 °C, 0.1 MPa) and shows large amounts of fibrillation

Table 3

Summary of penetrative impact performance by falling mass test comparing all-PP composites to alternative fibre reinforced PP composites (*impact properties of all-PP composites depend on processing conditions*)

Material	All-PP processing temperature (°C)	Conditions pressure (MPa)	Fibre weight fraction (%)	Density (g cm ⁻³)	Penetrative energy (J mm ⁻¹)	Specific penetrative energy (kJ g ⁻¹ mm ²)
All-PP	130	0.1	–	0.61	44.8	72.9
	150	0.1	–	0.61	44.8	73.7
	130	1.8	–	0.72	33.0	46.1
	150	1.8	–	0.77	28.2	36.8
	170	1.8	–	0.89	27.7	31.2
	130	11.4	–	0.85	21.4	25.3
	150	11.4	–	0.86	24.0	28.0
	170	11.4	–	0.91	25.2	27.6
Woven glass/PP	–	–	40	1.24	28.4	22.9
GMT	–	–	23	1.07	9.8	9.2
NMT	–	–	40	1.15	4.5	3.9

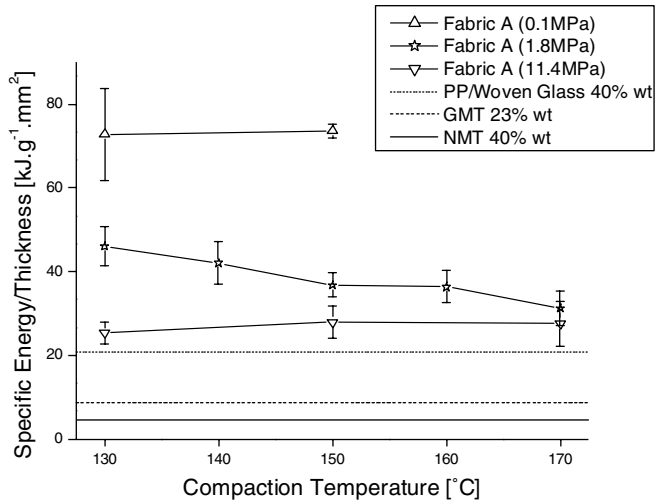


Fig. 9. Specific impact energy for different compaction pressures vs. compaction temperature (normalised for density). Since all-PP composites consolidated with the lowest compaction pressure also possess the lowest density, the specific energy absorption is far superior to the alternative reinforced PP systems compared here.

and delamination, and a higher overall energy absorption. Fig. 10b shows a similar specimen which has been processed at high temperature and pressure (160 °C, 11.4 MPa) and shows a characteristic ‘star’-shaped penetration which is formed by tape breakage and tearing along tape boundaries. This is a lower, more localised energy absorption, since the deformation is limited to the immediate impact site, unlike the specimen compacted at 140 °C, 0.1 MPa which shows larger deformations in the plane of the specimen, in the area surrounding the impact site.

Ignoring frictional losses, the energy absorbed upon falling weight impact, E_{total} , can be considered as follows:

$$E_{total} = E_T + E_I, \quad (3)$$

where E_T = energy absorbed by plastic tape deformation, E_I = energy absorbed by interfacial failure. The energy absorbed by tape deformation, E_T , will be dictated by the tensile behaviour of the composite. Since penetration requires tape failure, the energy absorption during impact can be compared to energy absorption during tensile testing of virgin tape and consolidated all-PP composites. If the impact load is considered to be solely absorbed by tapes that pass through the impact site, an effective volume of tape which is loaded upon impact can be calculated [48].

The effective tape volume can be modelled by considering the all-PP plate as stacked, unconsolidated tapes by ignoring interfacial properties and crimping, and solely considering tensile properties of the tape. Alternatively, to account for the effect of tape interactions, crimping, and the effects of composite processing, the tensile properties of woven specimens tested in the 0°/90° direction can be considered [12,37]. In either case, the volume loaded in tension can be considered as two rectangular sections running normal to one another with the impact site at the centre (see Fig. 11). Although the strain rate applied in impact (10^{-2} – 10^{-3} s⁻¹) is greater than that applied in the tensile tests (2.5×10^{-4} s⁻¹), the tensile strength and modulus are relatively consistent ($\pm 15\%$) over the strain rates seen here [11,12], and so absorbed energy is assumed to be similar.

Since impact energies are normalised for specimen thickness, specimen thickness can be ignored, and rather than considering effective tape volume, the effective tape area, A_{ET} , can be given by

$$A_{ET} = 2abV_fV'_f, \quad (4)$$

where a = striker diameter, 20 mm, b = effective tape length, 60 mm, V_f = volume fraction of tape in composite ≈ 1 , and V'_f = volume fraction of effective material in loading direction. To model impact based on the tensile behaviour

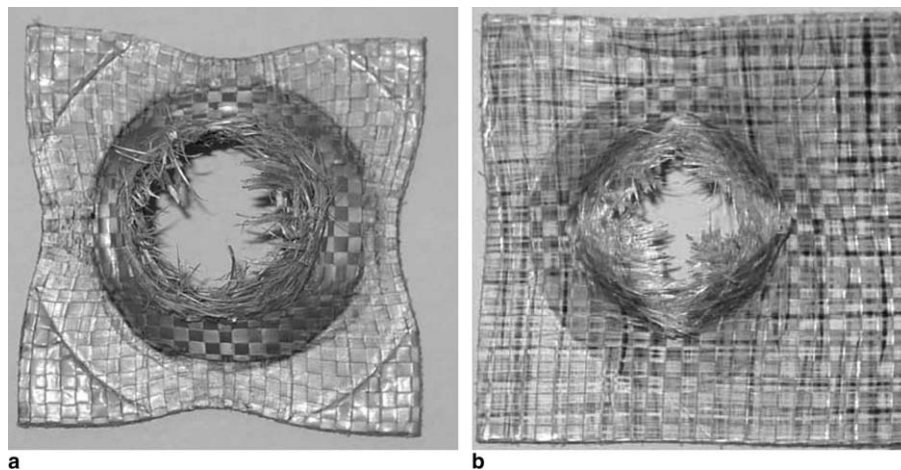


Fig. 10. Typical impact penetration damage at different compaction temperatures and pressures. Specimen (a) consolidated at lower temperature and pressure (140 °C, 0.1 MPa), shows large amounts of fibrillation and delocalised deformation giving a circular hole, while specimen (b) consolidated at higher temperature and pressure (160 °C, 11.4 MPa) shows very localised damage and breakage along tape boundaries giving a characteristic star-shaped hole.

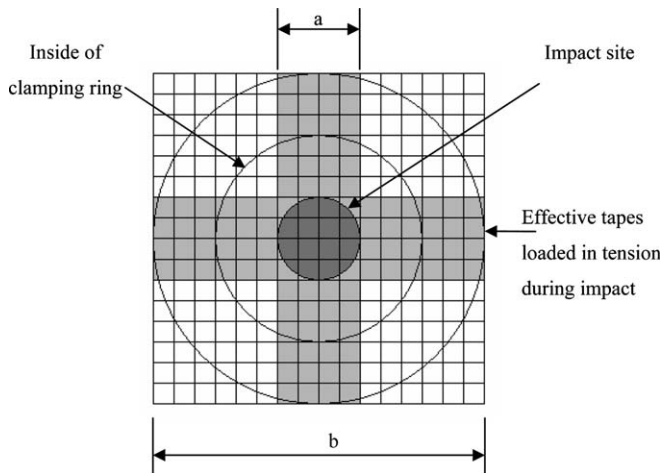


Fig. 11. Schematic of effective area of tapes loaded in tension during impact.

of stacked, unconsolidated tapes, $V'_f = 0.5$ since half of the tapes will be running normal to the direction of loading, and so make no contribution to tensile energy absorption. To model impact based on the tensile behaviour of compacted woven tape plies, $V'_f = 1$, since the tensile behaviour of the woven tape composite already accounts for ineffective tapes in the fabric oriented at 90° to the loading direction. Table 4 shows the energy absorbed by tensile failure of the tape together with woven tape composite tensile specimens obtained by integrating the area under stress vs. strains curves obtained during tensile testing. Combin-

ing this data with the energy absorbed by penetrative impact (see Fig. 12), shows that the energy absorbed solely by tensile failure of tapes is very close to the energy absorbed by impact failure of a woven tape composite specimen compacted 160°C and 11.4 MPa , of which 96% can be attributed to tape failure. However, the composite plate specimen compacted at 140°C and 0.1 MPa shows much greater energy absorption than can be solely attributed to tensile failure of the tapes, which in this case is only 27%. Since composite plates processed under this combination of low pressure and temperature possess much lower interfacial strengths, it is clear that here a large amount of energy is absorbed by tape pull-out or debonding. It is likely that the combination of a weak interface with stiff, strong tapes has a synergistic effect on the energy absorption of all-PP composites during impact, by allowing distribution of impact loading to a greater volume of tape. The fibre or tape pull-out is clearly visible from the difference in out of plane deformation of the two samples, as shown in Fig. 12.

It is worth noting, that although one can optimise absorbed impact energy through the control of the interface, this may result in a composite that has such poor interfacial strength that it may be unsuitable for some structural applications. However, this shows that composites properties can be tailored through the interface in the final processing step to suit the composite application. This is a unique feature of all-PP composites compared to traditional composites which often have fibre–matrix interaction which cannot be altered during production.

Table 4
Energy absorption mechanism of all-PP composites

Specimen	Tape	Compacted plate	
Compaction temperature ($^\circ\text{C}$)	–	140	160
Compaction pressure (MPa)	–	0.1	11.4
Energy absorbed by impact failure (per unit thickness) (J m^{-1})	–	4.5×10^4	2.5×10^4
Energy absorbed by tensile failure (J m^{-3})	2.3×10^7	5.2×10^6	1.0×10^7
Effective impact area loaded in tension (m^2)	1.2×10^{-3}	2.4×10^{-3}	2.4×10^{-3}
Energy absorbed by tape in effective impact area (per unit thickness) (J m^{-1})	2.7×10^4	1.2×10^4	2.4×10^4
Percentage of impact energy absorbed by tape failure	–	27%	96%

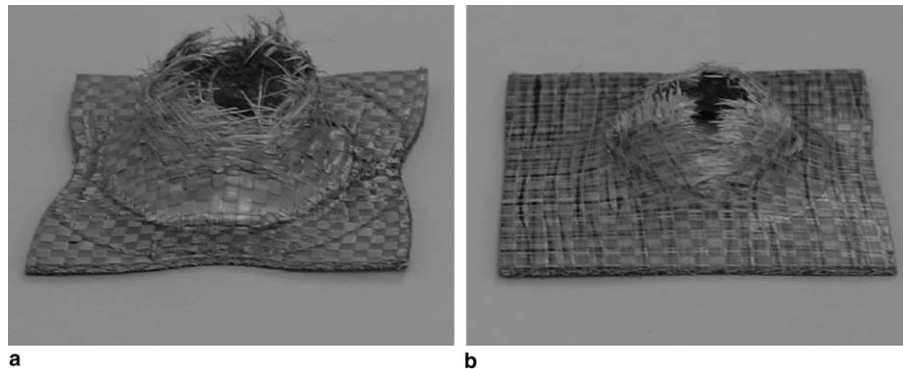


Fig. 12. Illustration of the out of plane deformation of all-PP composites. Specimen (a) consolidated at lower temperature and pressure (140°C , 0.1 MPa), shows large amounts out of plane deformation and tape pull through, while specimen (b) consolidated at higher temperature and pressure (160°C , 11.4 MPa) shows very localised damage and limited out of plane deformation.

3.2. Analysis of non-penetrative falling weight impact damage

In order to assess the damage tolerance of all-PP composites, non-penetrating impact tests were performed on a range of specimens manufactured from fabric A with three different compaction temperatures, but constant pressure (4 MPa). These specimens were impacted with 20 J and the compressive and tensile plastic surface strains were analysed with an ARAMIS digital optical strain mapping system. The major surface strains on the tensile (opposite to impacted) side due to the impact were compared and are presented in Figs. 13a, 13b and 13c and for the compressive (impacted) side in Figs. 17a, 17b and 17c. The processing temperatures of specimens in these images are shown in Table 5. Some of these strain maps show discontinuities of strain (shown as holes in the diagrams) which are due to either surface damage (tensile side) or removal of surface pattern due to abrasion of the striker upon impact (compressive side). Clearly visible on all images is also the circular pattern of the specimen clamp; this is shown as either a ring of high strain due to surface deformation,

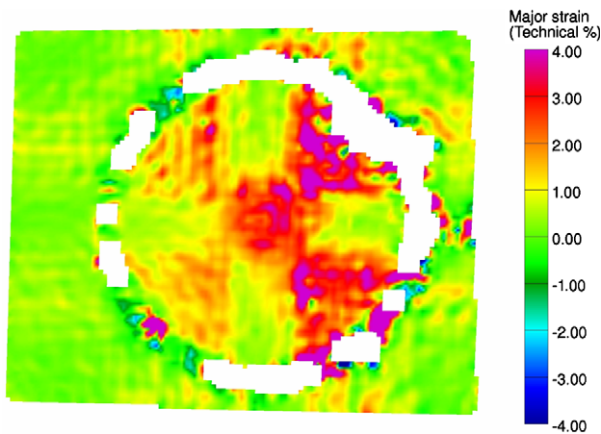


Fig. 13a. Tensile surface of all-PP plate compacted at 125 °C and impacted with 20 J.

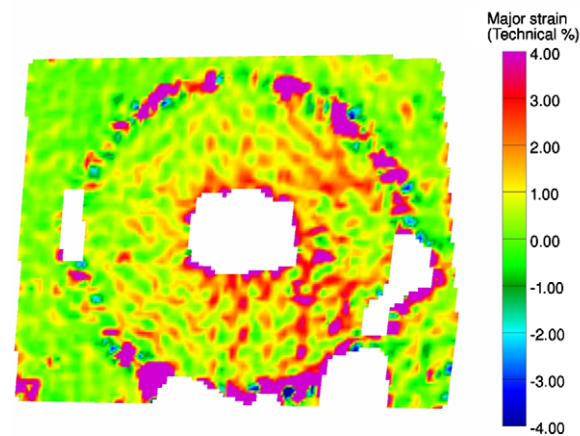


Fig. 13b. Tensile surface of all-PP plate compacted at 140 °C and impacted with 20 J.

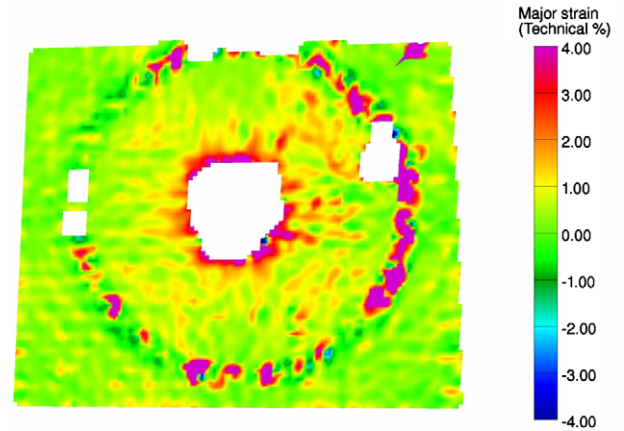


Fig. 13c. Tensile surface of all-PP plate compacted at 160 °C and impacted with 20 J.

Table 5
Summary of non-penetrative impact specimen figures

Compaction temperature (°C)	Impact energy (J)	Figure	
		Tensile face	Compressive face
125	20	13a	17a
140	20	13b	17b
160	20	13c	17c

or by discontinuous strain mapping due to removal of the surface pattern by the clamp. In all the strain mapping sections detailed below, specimens are oriented with tapes running approximately horizontally and vertically in the plane of the page.

Figs. 13a, 13b and 13c show a range of damage processes for the specimens compacted at 125, 140 and 160 °C, respectively, and subjected to a 20 J impact. As compaction temperature increases from 125 to 160 °C there is a transition from anisotropic behaviour to a more isotropic state, and the areas of greatest strain are located in regions at $\pm 45^\circ$ to the tape directions. This is because the tensile modulus of composites loaded in the $\pm 45^\circ$ direction is approximately 40% to that of the 0° (tape) direction [37], so stress in this direction is much more easily relieved by deformation through interply shearing. This is illustrated in Fig. 14. Fig. 15 shows the stress/strain curves of two consolidated woven fabric plates compacted at 140 and 160 °C, and tested at $0^\circ/90^\circ$ and $\pm 45^\circ$ to the tape direction. This illustrates the difference in moduli, but also the difference in elastic limits of $0^\circ/90^\circ$ and $\pm 45^\circ$ specimens. It is likely that there is some strain in the 0° and 90° direction tapes in the impacted plate, but this is elastic strain which is dissipated in the rebound of the striker, and not visible in the post impact specimens, whereas the strain in the $\pm 45^\circ$ direction to the tapes is plastic and so is seen in the post impact strain map.

This directional change in modulus is also affected by compaction temperature; specimens compacted at 125 °C possess poor interfacial bonding and thus surface tapes will be much freer to shear (the ‘trellis’ effect [49]), than those

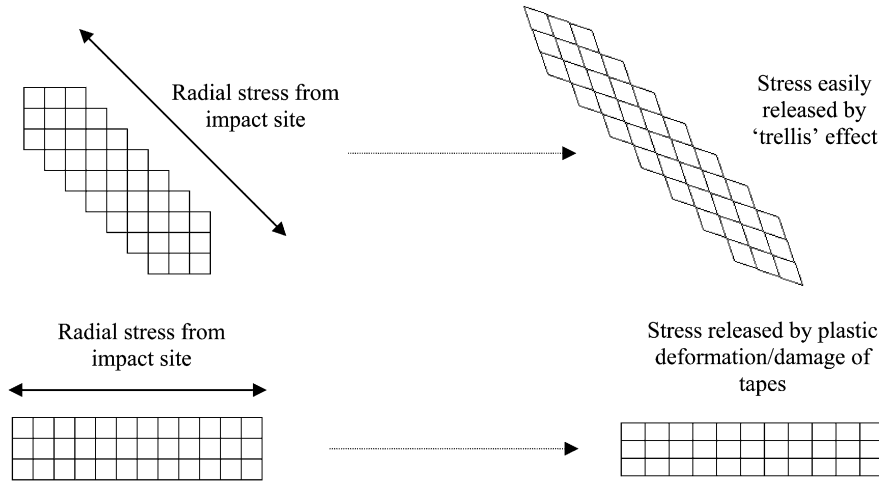


Fig. 14. Stress dispersion in different angles to tape direction showing the ease of plastic deformation during loading at $\pm 45^\circ$ to tape direction.

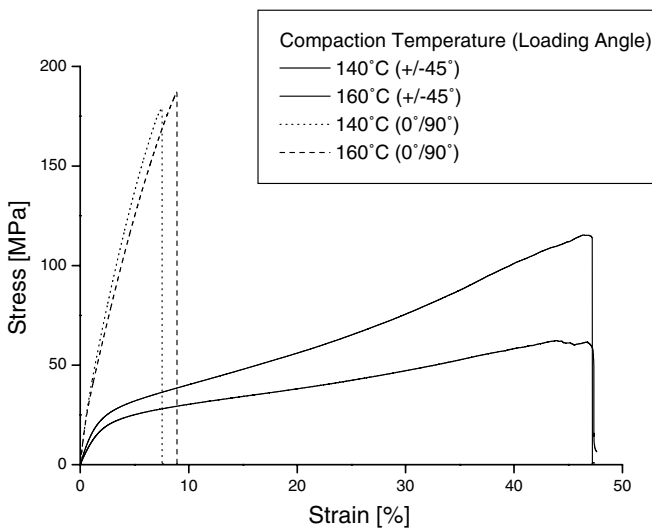


Fig. 15. Typical stress vs. strain curves for woven tape composite specimens loaded in tension at $0^\circ/90^\circ$ and $\pm 45^\circ$ to tape direction, showing greater plastic deformation of specimens loaded at $\pm 45^\circ$ to tape direction.

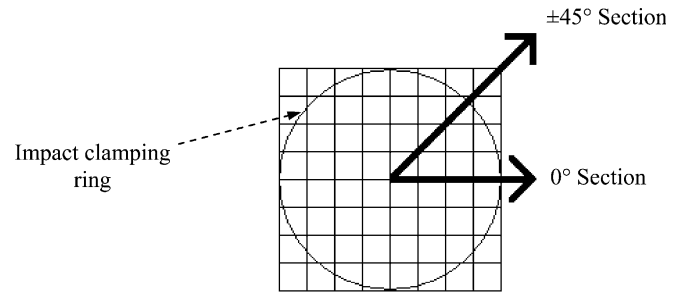


Fig. 16. Illustrating orientation of strain sections shown in Figs. 18 and 19.

Figs. 17a, 17b and 17c show specimens which have been compacted at 125, 140 and 160 °C, respectively, and subjected to a 20 J impact. These show a similar situation as for the tensile side of the impact (see Figs. 13a, 13b and 13c), but now even at the compaction temperature of 160 °C, the strain distribution is inhomogeneous, and is cross-shaped due to the anisotropy of the system. As compaction temperature, and so interfacial strength, increases,

compacted at 160 °C which will be much more firmly locked in position. Thus increased compaction temperatures lead to a more homogenous system.

Fig. 18 illustrates the effect of the consolidation on the strain of the tensile surface of the laminates. The graph represents the major strain as a function of the radial distance from the centre of the impact site (20 mm is the radius of the clamped region) for two sections at 0° and $\pm 45^\circ$ to the tape direction (see Fig. 16). The specimen compacted at 125 °C shows that strain in the section radiating in the 0° direction decreases with increasing distance for impact site, as would be expected, but more importantly, much greater strains are seen in the section radiating at $\pm 45^\circ$ to the tape direction. This shows the heterogeneity of strain distribution in this specimen. Contrary to this, the specimen compacted at 160 °C shows very similar strain distribution whether a section is taken at 0° or $\pm 45^\circ$ to the tape direction.

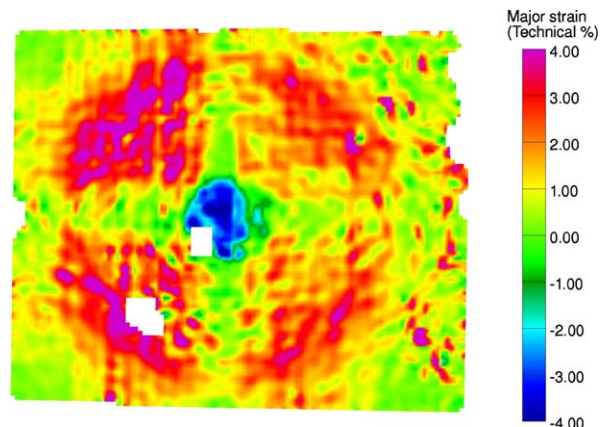


Fig. 17a. Compressive surface of all-PP plate compacted at 125 °C and impacted with 20 J.

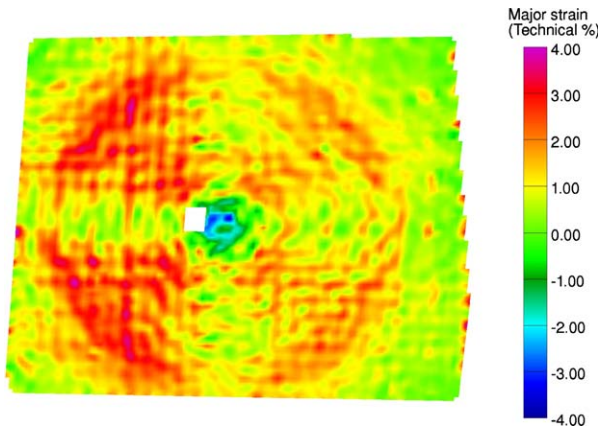


Fig. 17b. Compressive surface of all-PP plate compacted at 140 °C and impacted with 20 J.

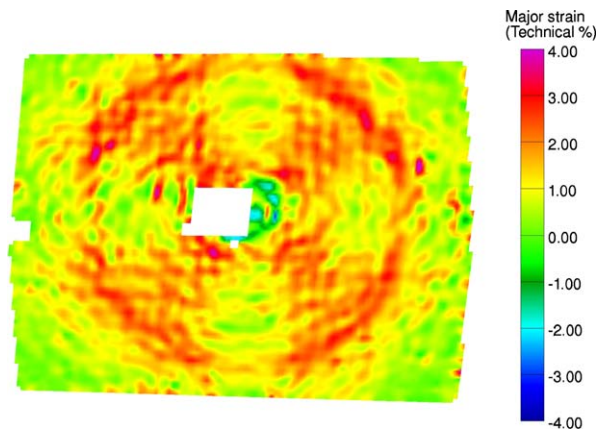


Fig. 17c. Compressive surface of all-PP plate compacted at 160 °C and impacted with 20 J.

the cross shape becomes less defined due to better load transfer between neighbouring tapes.

Like Fig. 18, Fig. 19 shows the strain distribution of 2 sections on the compression sides of two specimens, compacted with two different temperatures, and then impacted with 20 J. Again, a similar effect is seen, with 0° and ±45° sections having very much different magnitudes of strain for the specimen compacted at 125 °C, but are quite similar for the specimen compacted at 160 °C. The compressive region in the middle of the specimen is also seen in this graph as an area of negative (compressive) strain. From this, it can also be seen that the plastic deformation due to the striker at the impact site is much greater for the specimen compacted at 125 °C than at 160 °C. This implies that the specimen compacted at 125 °C, would have lower resistance to denting than the specimen compacted at 160 °C, despite a greater penetration resistance. This is an important consideration for applications in which the material has to be resistant to surface damage as well as providing penetrative protection. The oscillations seen in the strain magnitude for the specimen shown in Figs. 18 and 19, have a wavelength of approximately 4 mm, and this can be

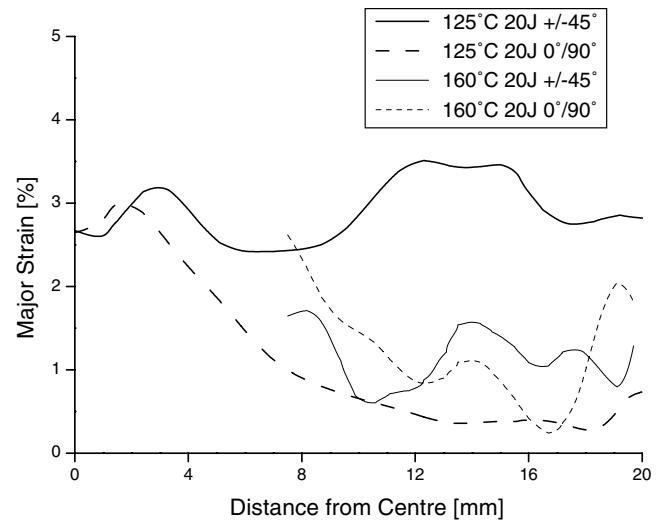


Fig. 18. Surface strain section of typical tensile face of impact specimen showing the change in major strain with increasing distance from impact centre in the ±45° and 0°/90° directions for specimens processed with two different temperatures.

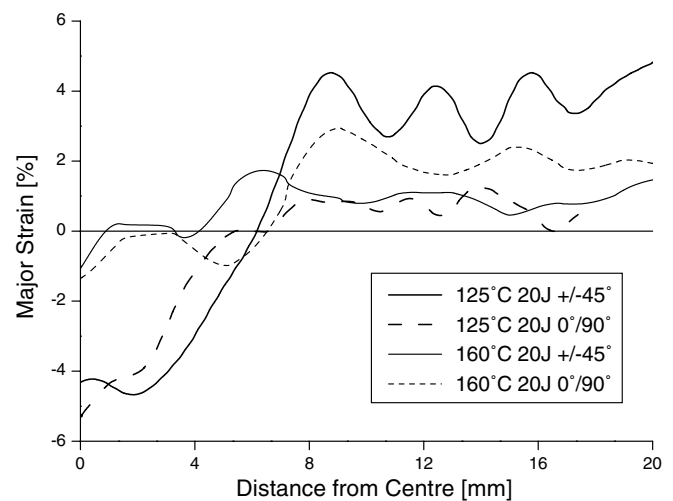


Fig. 19. Surface strain section of typical compressive face of impact specimen showing the change in major strain with increasing distance from impact centre in the ±45° and 0°/90° directions for specimens processed with two different temperatures. Clearly visible are oscillations which relate to the woven structure of the tape in the fabric.

explained by the fact that the strain is calculated on the surface of a woven fabric, with each tape being approximately 2 mm wide. The peaks in the strain represent the tapes in the 0° direction which are running radially from the impact site in the 0° direction. The tapes which are perpendicular to these are not directly loaded and so show much lower strain. The specimen compacted at 160 °C shows much less oscillation due to the increased bonding and superior load transfer as described above.

The use of optical strain mapping only provides information about surface strains, and since compressive and tensile faces show different strain situations, it is likely that while the surface strains indicate the through-thickness

Table 6
Summary of the effect of processing conditions on impact properties of all-PP composites

Property	Increasing compaction temperature or pressure
Density	▲
Penetrative impact resistance	▼
Peel strength	▲
Uniformity of surface strain	▲

strain distribution, they cannot totally describe the strain distribution in a specimen. Since the outer surfaces of the specimen are gripped during impact, it is likely that greater strain is present in sub-surface plies due to interply shearing following delamination. Thus information obtained by optical strain mapping must be considered as an indicative rather than an exhaustive description of the strain distribution, and thus energy absorption of a specimen.

4. Conclusions

The impact performance of all-PP composite materials has been analysed through penetrating and non-penetrating impact by falling weight testing. From these results, some conclusions may be made; all-PP composite plates possess excellent resistance to falling weight impact penetration and can compete or outperform glass or natural fibre reinforced polypropylene (see Table 3). The dominant failure modes of all-PP composites in impact are delamination and tape fracture. Since the interfacial strength of all-PP composites is controlled by processing conditions, it is possible to tailor the impact resistance by altering tape production parameters or composite compaction parameters. Impact performance increases with decreasing interfacial strength, with penetration energy increasing with decreasing compaction temperature and pressure. All-PP composites which are optimised for impact, however, may not possess adequate interfacial strengths to make them viable structural components. Alternatively, such all-PP composites may find applications as low-cost alternatives to current rigid impact protection materials which are aimed at protection from low velocity impacts. A summary of the impact properties of all-PP composites plates is shown in Table 6.

Acknowledgements

The co-extruded PP tapes used in this study were prepared using facilities at Lankhorst Indutech BV, Netherlands. This work was sponsored by the Dutch Government's Economy, Ecology and Technology (EET) programme for sustainable development, under Grant No. EETK97104.

References

[1] Richardson MOW, Wisheart MJ. Review of low-velocity impact properties of composite materials. *Composites: Part A* 1996;27A:1123–31.

[2] Bigg DM. The impact behavior of thermoplastic sheet composite. *J Reinf Plast Compos* 1994;13:339–54.

[3] Jacobs MJN, van Dingenen JJJ. Ballistic protection mechanisms in personal armour. *J Mater Sci* 2001;36:3137–42.

[4] Beugels J. Lightweight high performance Dyneema Spall-liners in armoured military vehicles. In: *Lightweight armour system symposium*; 2001.

[5] Tarim N, Findik F, Uzun H. Ballistic impact performance of composite structures. *Compos Struct* 2001;56:13–20.

[6] Findik F, Tarim N. Ballistic impact efficiency of polymer composites. *Compos Struct* 2003;61:187–92.

[7] Shockey DA, Erlich DC, Simmons JW. Lightweight fragment barriers for commercial aircraft. In: *18th International symposium on ballistics*; 1999.

[8] Dean G, Wright L. An evaluation of the use of finite element analysis for predicting the deformation of plastics under impact loading. *Polym Test* 2003;22:625–31.

[9] Morye SS, Hine PJ, Duckett RA, Carr DJ, Ward IM. Modelling of the energy absorption of polymer composites upon ballistic impact. *Compos Sci Technol* 2000;60:2631–42.

[10] Schimanski T. PhD thesis, Technische Universiteit Eindhoven, Netherlands; 2002.

[11] Alcock B. PhD thesis, Queen Mary, University of London, UK; 2004.

[12] Cabrera N. PhD thesis, Technische Universiteit Eindhoven, Netherlands; 2004.

[13] Carothers WH, Hill JW. Studies of polymerization and ring formation. XV. Artificial fibres from synthetic linear condensation superpolymers. *J Am Chem Soc* 1932;54:1579–87.

[14] Takayanagi M, Imada K, Kajiyama T. Mechanical properties of fine structures and drawn polymers. *J Polym Sci: Part C* 1966;15:263–81.

[15] Aharoni SM, Sibilija JP. Crystalline transitions and the solid state extrusion of polymers. *J Appl Polym Sci* 1979;23:133–40.

[16] Aharoni SM, Sibilija JP. On the conformational behavior and solid-state extrudability of crystalline polymers. *Polym Eng Sci* 1979;19:450–5.

[17] Wills AJ, Capaccio G, Ward IM. Plastic deformation of polypropylene: effect of molecular weight on drawing behavior and structural characteristics of ultra-high modulus products. *J Polym Sci: Polym Phys Ed* 1980;18:493–509.

[18] Yamada K, Kamezawa M, Takayanagi M. Relationship between orientation of amorphous chains and modulus in highly oriented polypropylene. *J Appl Polym Sci* 1981;26:49–60.

[19] Takayanagi M, Yamada K. Analysis of zone-drawing process in preoriented polypropylene. *J Appl Polym Sci* 1982;27:2091.

[20] Burke PE, Weatherley GC, Woodhams RT. Uniaxial roll-drawing of isotactic polypropylene sheet. *Polym Eng Sci* 1987;27:518–23.

[21] Yang J, Chaffey CE, Vancso GJ. Structure, transitions, and mechanical properties of polypropylene oriented by roll-drawing. *Plast Rubber Compos Process Appl* 1994;21:201–10.

[22] Loos J, Schimanski T, Hofman J, Peijs T, Lemstra PJ. Morphological investigation of polypropylene single-fibre reinforced polypropylene model composites. *Polymer* 2001;42:3827–34.

[23] Bartczak Z, Moraweic J, Galeski A. Structure and properties of isotactic polypropylene oriented by rolling with side constraints. *J Appl Polym Sci* 2002;86:1413–25.

[24] Capiati NJ, Porter RS. The concept of one polymer composites modelled with high density polyethylenes. *J Mater Sci* 1975;10:1671–7.

[25] Mead TW, Porter RS. Annealing characteristics of ultraoriented high-density polyethylene. *J Appl Phys* 1976;47:4278–88.

[26] Chand N, Kreuzberger S, Hinrichsen G. Influence of processing conditions on the tensile properties of unidirectional UHMPE fibre/LDPE composites. *Composites* 1993;25:878–90.

[27] Rasburn J, Hine PJ, Ward IM, Olley RH, Bassett DC, et al. The hot compaction of polyethylene terephthalate. *J Mater Sci* 1995;30:615–22.

[28] Wright DD, Lautenschlager EP, Gilbert JL. Bending and fracture toughness of woven self-reinforced composite poly(methyl methacrylate). *J Biomed Mater Res* 1996;36:441–53.

- [29] Abo El-Maaty MI, Bassett DC, Olley RH, Hine PJ, Ward IM. The hot compaction of polypropylene fibres. *J Mater Sci* 1996;31:1157–63.
- [30] Lacroix F, Werwer M, Schulte K. Solution impregnation of polyethylene fibre/polyethylene matrix composites. *Composites: Part A* 1998;29:371–6.
- [31] Lacroix F, Loos J, Schulte K. Morphological investigations of polyethylene fibre reinforced polyethylene. *Polymer* 1999;40:843–7.
- [32] Hine PJ, Ward IM, Jordan ND, Olley RH, Bassett DC. A comparison of the hot-compaction behavior of oriented, high-modulus, polyethylene fibers and tapes. *J Macromol Sci: Physics* 2001;B(40):959–89.
- [33] Ward IM, Hine PJ. The science and technology of hot compaction. *Polymer* 2004;45:1413–27.
- [34] Olley RH, Bassett DC, Hine PJ, Ward IM. Morphology of compacted polyethylene fibres. *J Mater Sci* 1993;28:1107–12.
- [35] Jordan ND, Bassett DC, Olley RH, Hine PJ, Ward IM. The hot compaction behaviour of woven oriented polypropylene fibres and tapes. II. Morphology of cloths before and after compaction. *Polymer* 2003;44:1133–43.
- [36] Hine PJ, Ward IM, Jordan ND, Olley RH, Bassett DC. The hot compaction behaviour of woven oriented polypropylene fibres and tapes. I. Mechanical properties. *Polymer* 2003;44:1117–31.
- [37] Alcock B, Cabrera N, Barkoula N-M, Loos J, Peijs T. The mechanical properties of woven tape all-polypropylene composites. *Composites: Part A* 2005 [submitted for publication].
- [38] Alcock B, Cabrera N, Barkoula N-M, Loos J, Peijs T. The mechanical properties of unidirectional all-polypropylene composites. *Composites: Part A* 2005 [accepted].
- [39] Peijs T. *Mater Today* 2003;April:30–5.
- [40] Bastiaansen CWM, Lemstra PJ. Melting behaviour of gel-spun/drawn polyolefins. *Macromol Symp* 1989;28:73–84.
- [41] Barkoula N-M, Schimanski T, Loos J, Peijs T. Processing of single polymer composites using the concept of constrained fibers. *Polym Compos* 2004;26:114–20.
- [42] Kalthoff JF. On the validity of impact energies measured with polymeric specimens in instrumented impact tests. *Impact Dynamic Fract Polym Compos ESIS* 1993;19.
- [43] ISO Standard 6603-2. *Plastics – Determination of multi-axial impact behaviour of rigid plastics*. 1989.
- [44] Tyson J, Schmidt T, Galanulis K. Advanced photogrammetry for robust deformation and strain measurement. In: *Proceedings of SEM 2002 annual conference*; 2002.
- [45] Martin TA, Christie GR, Bhattacharyya D. Grid strain analysis and its application in composite sheet forming. In: Bhattacharyya D, editor. *Composite sheet forming*; 1997 [Chapter 6].
- [46] Harel H, Marom G, Kenig S. Delamination controlled ballistic resistance of polyethylene/polyethylene composite materials. *Appl Compos Mater* 2002;9:33–42.
- [47] Morye SS, Hine PJ, Duckett RA, Carr DJ, Ward IM. A comparison of the properties of hot compacted gel-spun polyethylene fibre composites with conventional gel-spun polyethylene fibre. *Composites: Part A* 1999;30:649–60.
- [48] Peijs T, Smets EAM, Govaert LE. Strain rate and temperature effects on energy absorption of polyethylene fibres and composites. *Appl Compos Mater* 1994;1:35–54.
- [49] Cutolo D, Savadori A. Processing of product forms for the large-scale manufacturing of advanced thermoplastic composites. *Polym Adv Technol* 1994;5:545–53.
- [50] Dwight DW. Glass fiber reinforcement. In: Kelly A, Zweben C, editors. *Comprehensive composite materials*; 2000.
- [51] Yang HH. Aramid fibers. In: Kelly A, Zweben C, editors. *Comprehensive composite materials*; 2000.
- [52] Peijs T, Jacobs MJN, Lemstra PJ. High performance polyethylene fibres. In: Kelly A, Zweben C, editors. *Comprehensive composite materials*; 2000.
- [53] Hine PJ, Ward IM, Olley RH, Bassett DC. The hot compaction of high modulus melt-spun polyethylene fibres. *J Mater Sci* 1993;28:316–24.
- [54] Darras O, Duckett RA, Hine PJ, Ward IM. Anisotropic elasticity of oriented polyethylene materials. *Compos Sci Technol* 1995;55:131–8.
- [55] Yan PJ, Hine PJ, Ward IM, Olley RH, Bassett DC. The hot compaction of spectra gel-spun polyethylene fibre. *J Mater Sci* 1997;32:4821–31.
- [56] Kristiansen M, Tervoort T, Smith P. Synergistic gelation of solutions of isotactic polypropylene and bis-(3,4-dimethyl benzylidene) sorbitol and its use in gel-processing. *Polymer* 2003;44:5885–91.